A solar-powered hand-launchable UAV for low-altitude multi-day continuous flight

Philipp Oettershagen[1], Amir Melzer, Thomas Mantel, Konrad Rudin,
Rainer Lotz, Dieter Siebenmann, Stefan Leutenegger, Konstantinos Alexis and Roland Siegwart

***Abstract*— Abstract. Idea for this paper:**
- Conceptual design, realization/integration, development of onboard systems, flight testing and verification of conceptual/preliminary design =¿ Complete cycle including all steps can be shown here. - Demonstrations -¿ rather basic control approaches chosen, i.e. this platform will be the basis for further research in control, guidance & navigation, mapping and will go towards the applications of XXX - solar-powered, hand-launchable 5m-class Unmanned Aerial Vehicle with multi-day continuous flight capability combined with payload capacity for long-endurance SAR and inspection missions. Questions: - This paper = engineering paper, rest is then BASING upon this paper (use it as a ref). Is this OK? Is the chance that this will be accepted big enough? -¿ Yes, focus on "complete cycle" here, with more details in papers XXX to YYY - We ware special : mission applications possible, long endurance, combination

I. INTRODUCTION

A. Solar-powered UAVs for perpetual flight endurance

When carefully designed, solar-electrically powered fixed-wing Unmanned Aerial Vehicles (UAVs) exhibit significantly increased flight endurance over purely-electrically or even gas-powered aerial vehicles. Given certain environmental conditions, a solar-powered UAV creates surplus energy when observed over a full day-night cycle, i.e. it will fully recharge its batteries during the day to continue flight through the night and potentially subsequent day-night cycles. Long endurance - and especially this multi-day continuous flight capability termed "perpetual endurance" - is of significant interest for large-scale mapping, observation or telecommunications relay applications as they occur in Search-And-Rescue (SAR) missions, industrial or agricultural inspection, meteorological surveys, border patrol and more [**?**].

Recently, interest in employing solar-powered large-scale (wing span above 20m) High-Altitude Long-Endurance (HALE) UAVs as "atmospheric satellites" - i.e. stationary/loitering platforms e.g. for telecommunications relay - has peaked. Notable examples of this trend are Solara [**?**] and Zephyr, the latter of which has already demonstrated a continuous flight of 14 days[**?**]. In contrast, smaller scale solar-powered UAVs are mostly designed for Low-Altitude Long Endurance (LALE) applications. While they have to cope with the more challenging meteorological phenomenas of the lower atmosphere (clouds, rain, wind gusts or thermals), they generally have the advantage of lower complexity and cost as well as easier and faster handling (e.g. through hand-launchability) as beneficial in First-Aid SAR scenarios. However, research in small-scale solar UAVs targeting perpetual endurance has been relatively sparse, with most research including [**?**] focussing on conceptual design studies without extensive flight experience. However, in 2005, Cocconi's SoLong [**?**] performed a continuous 48 hours flight using solar power and thermal-updraft hunting, though with limited airplane autonomy. Noth[**?**] presents the conceptual design methods, realization and experimental flight results of the 3.2m wing span "SkySailor", which demonstrated a 27 hours solar-powered continuous flight without the use of thermals in 2008.

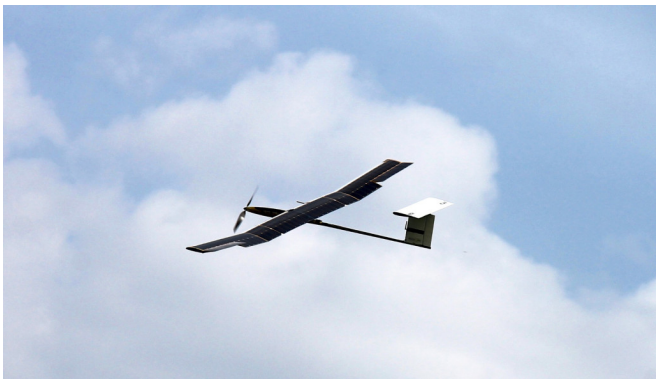

Fig. 1. The AtlantikSolar solar-powered UAV developed at ETH Zurich

B. Contributions of this paper

This paper aims to extend the work of [**?**], [**?**] by presenting AtlantikSolar, a solar-powered LALE-UAV with a wing span of 5.6m designed towards more robust multi-day autonomous operation capabilities while providing the option to use an advanced optical&infrared sensor system together with on-board computation ressources developed at ETH Zurich. The contribution of the paper lies in presenting the complete development cycle from conceptual UAV design to actual testing and missions, or more specifically

1) The application and extension of the conceptual design approach in [**?**], [**?**] towards more robust multi-day flight under sub-optimal meteorological conditions
2) The realization of the conceptual design in UAV hardware, i.e. structure, low-level electronics & avionics

All authors are part of the Autonomous Systems Lab, Swiss Federal Institute of Technology Zurich (ETH Zurich). Leonhardstrasse 21, 8092 Zurich, Switzerland.
[1] E-Mail:philipp.oettershagen@mavt.ethz.ch
*This work was supported by a number of project partners and generous individuals, see http://www.atlantiksolar.ethz.ch/

3) The development of onboard EKF state estimation algorithms and flight control methods based on PID control with non-linear guidance
4) The discussion of flight test results including long-endurance flight (up to 12h) and mapping results during exemplary Search-And-Rescue missions.

II. CONCEPTUAL DESIGN

A. Methodology

The conceptual design methodology for solar-powered UAVs used in this paper was developed at ETH Zurich by [**?**], [**?**] and is briefly summarized below. To analyze flight performance and a potential perpetual flight capability, the energy input/output-balance needs to be modeled. The total required nominal electrical output power

$$P_{out}^{nom} = \frac{P_{level}}{\eta_{prop}} + P_{av} + P_{pld} \tag{1}$$

consists of the required electrical propulsion power for level-flight $\frac{P_{level}}{\eta_{prop}}$, where η_{prop} includes propeller, gearbox, motor, and motor-controller efficiency, and the necessary avionics and payload power P_{av} and P_{pld}. The aircraft is assumed to fly at the airspeed of minimum aerodynamic level-flight power

$$P_{level} = \left(\frac{C_D}{C_L^{\frac{3}{2}}}\right)_{min} \sqrt{\frac{2(m_{tot}g)^3}{\rho(h)A_{wing}}}. \tag{2}$$

Here, $m_{tot} = m_{bat}+m_{struct}+m_{prop}+m_{sm}+m_{av}+m_{pld}$ is the total airplane mass, where structure, propulsion and solar module masses $m_{struct}, m_{prop}, m_{sm}$ are automatically sized according to [**?**], [**?**] and m_{av}, m_{pld} are given in table I. The local earth gravity is designated by g, A_{wing} is the wing area, and rho is air density. The airplane lift and drag coefficients C_L and C_D are retrieved from 2-D airfoil simulations using XFoil [**?**], with C_D being combined with parasitic drag from the airplane fuselage and stabilizers and the induced drag

$$C_{D,ind} = \frac{c_L^2}{\pi \cdot e_0 \cdot \lambda}. \tag{3}$$

Here, $e_0 \approx 0.92$ is the Oswald efficiency and λ the wing aspect ratio. On the input side, the nominal solar input power

$$P_{solar}^{nom} = I \cdot A_{sm} \cdot \eta_{sm} \cdot \eta_{mppt} \tag{4}$$

considers the solar module area $A_{sm} = f_{sm} \cdot A_{wing}$ with relative fill-factor f_{sm}, module efficiency η_{sm}, and Maximum Power Point Tracker (MPPT) efficiency η_{mppt}. The solar radiation $I = I(\varphi, h, t)$ is assumed to be a function of the geographical latitude φ, the altitude h, and the current date and local time t, and is modeled as in [**?**]. The state equation can now be formulated in a simplified form as

$$\begin{aligned} \frac{dE_{bat}}{dt} &= P_{solar}(\varphi, h, t) - u - P_{av} - P_{pld}, \\ \frac{dh}{dt} &= \frac{\eta_{prop} \cdot u - P_{level}(h)}{m_{tot} g}. \end{aligned} \tag{5}$$

Here, u is the actual electrical power sent to the propulsion system. Simple forward integration of the state equation (5) gives the battery state of charge (SoC) over time and thus determines the perpetual flight capability.

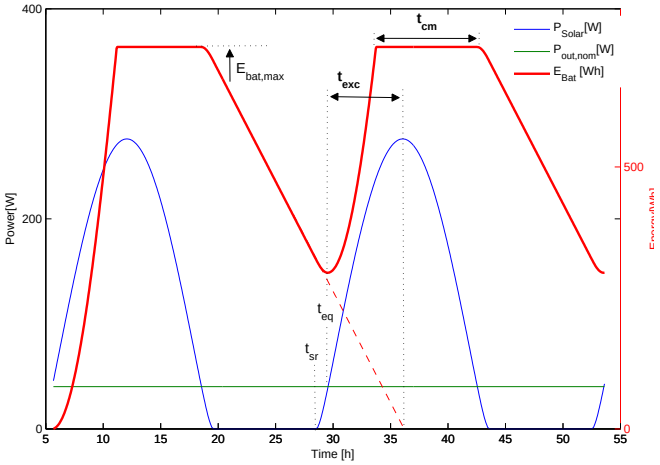

Fig. 2. Energetic simulation of the AtlantikSolar UAV configuration ($b = 5.6m$, $\lambda = 18.5$, $m_{bat} = 3.5kg$), showing input and output power, battery capacity, and performance metrics excess time t_{exc} and charge margin t_{cm} during a 2-day flight.

For the design optimization, we assume that a solar-powered UAV configuration is designed for missions at and around a specific date of the year (DoY) and geographical latitude φ, and thus φ and DoY are fixed parameters. The three design parameters to be optimized are

- The wingspan b and wing aspect ratio λ, which specify wing geometry and thus influence the level-power in (2) and the solar input power in (4).
- The battery mass m_{bat} contained in m_{tot} in (2)

B. Extension of conceptual design optimization criteria

The conceptual design tool developed in [**?**], [**?**] has been extended in two ways: First, it now provides the capability to perform energetic simulations of multi-day solar-powered flight, whereas before only one day-night cycle was considered. Fig. 2 shows the results for incoming solar power P_{solar}, required power P_{out}, and remaining battery charge E_{bat} obtained for a two day/night cycle flight. Clearly, the initial charge condition E_{bat} at time of sunrise $t_{sr} = min(t(P_{solar} > 0))$ for the second day is different than on the first day, which significantly reduces the required charge time until $E_{bat} = E_{bat}^{max}$ and leads to increased charge margins with respect to the pure one day/night-cycle simulation. Second, and more importantly, the optimization criteria are extended with respect to [**?**], [**?**] to achieve more robust multi-day flight. In general, a necessary and sufficient condition for perpetual flight is that the excess time $t_{exc} > 0$, where

$$t_{exc} = \frac{E_{bat}(t = t_{eq})}{P_{out}^{nom}} \Big| P_{solar}(t > t_{sr}) = 0 \tag{6}$$

with "power-equality time" $t_{eq} = t(P_{solar}^{nom} = P_{out}^{nom})$ in the morning. This means that at $t = t_{eq}$ there has to exist remaining battery capacity to continue flight e.g. in case of cloud coverage in the morning. This is why[**?**], [**?**] focus on maximizing t_{exc}. However, a large t_{exc} does not provide direct robustness against disturbances in P_{solar}

during the charging process(e.g. due to clouds). In contrast, when optimizing purely for t_{exc}, the methodology in Sec. II-A will select the largest battery size (due to the scaling of P_{level} with m_{bat}) which can still be fully charged unter optimal conditions, but every reduction in P_{solar} will directly decrease t_{exc} due to only partially charged batteries. We thus introduce the charge margin t_{cm} as the time margin between achieving the full charge $E_{bat} = E_{bat}^{max}$ and restart of the discharge in the evening. In case of decreased solar power income, $t_{cm} > 0$ will provide an additional margin before a decrease in excess time occurs.

The overall approach for increasing robustness with respect to local disturbances in the power income and output is thus to determine the lowest acceptable t_{exc} satisfying the UAV application requirements, and to then optimize the configuration for t_{cm}. The exact procedure applied here is:

1) Choose the nominal operating latitude φ and Day-of-Operation DoY^{nom}, and the outermost days where perpetual UAV endurance is required $DoY^{min,max}$
2) Obtain t_{night}^{min} and t_{night}^{max} for the range of $DoY = [DoY^{min}, DoY^{max}]$ from [**?**].
3) The required excess time $t_{exc,req}$ is now the sum of
   - $t_{exc,DoY} = t_{night}^{max} - t_{night}^{min}$
   - $t_{exc,clouds}$, to allow a margin for clouds in the morning or evening
   - $t_{exc,P_{level}}$, to allow a margin for increased power consumption e.g. caused by downdrafts or uncertainties in estimating P_{level}
4) Perform the design analysis given the methodology in sec. II-A for $DoY(t_{night} = t_{night}^{min})$. Pre-select the subset $\mathcal{S}$ of configurations satisfying $t_{exc} > t_{exc,req}$.
5) Within $\mathcal{S}$, allow for a set of intermediate configurations $\mathcal{S}_i$ to take into account UAV-specific constraints on b, λ, or m_{bat}. Then choose the final configuration $\mathcal{S}_f$ from $\mathcal{S}_i$ to obtain the largest charge margin t_{cm}.

This conceptual design methodology is applied below. An alternative conceptual design approach utilizing a weighed version of t_{exc} and t_{cm} is proposed in [**?**].

C. Application of Conceptual Design methodology

AtlantikSolar operate at a nominal latitude of $\varphi = 45N$ and shall provide perpetual endurance within a +/-2 month window around DoY_{nom}=June 21st (April 21st-August 21st). From [**?**], we find $t_{night}^{min} = 8.7h$ (June 21st), $t_{night}^{max} = 10.5h$(April 21st), and thus $t_{exc,DoY} = 1.80h$. We choose $t_{exc,clouds} = 3.0h$ to account for three hours of full cloud coverage either on the evening or the morning and choose $t_{exc,P_{level}} = 0.2 \cdot t_{night,max} = 2.1h$ to cover increased power consumption due to modelling errors, downdrafts or headwinds. Using $t_{exc,req} = t_{exc,DoY} + t_{exc,clouds} + t_{exc,P_{level}}$, we retrieve $t_{exc,req} = 6.9h$ as the minimum required excess time for robust perpetual-flight at the given dates and locations.

The design methodology tool of section II-A is now applied assuming the fixed component performance parameters in Tab. I. Fig. 3 shows the resulting plot for t_{exc} versus the optimization variables b, m_{bat} and $\lambda = 18.5$. The subset $\mathcal{S}$ of configurations satisfying $t_{exc} > t_{exc,req}$ is the region within the blue contour-line. The optimum clearly occurs at large wing spans, however, considering an external size constraint (each of the three wing pieces of AtlantikSolar shall be $< 2m$ in wing span to allow proper handling and transport), we choose $b = 5.6m$. The aspect ratio $\lambda = 18.5$ is found to provide an optimum in t_{exc} and also allows to seamlessly integrate the solar cells (see Sec. III-A.1) inside the wing chord. The last design choice is now m_{bat}, for which we seek to optimize t_{cm} within the previously selected set $\mathcal{S}_i = (\mathcal{S}|b = 5.6m, \lambda = 18.5)$. As visible in Fig. 3, $m_{bat} = 3.0...7.5kg$ lie within $\mathcal{S}_i$. We choose $m_{bat} = 3.5kg$ to optimize t_{cm} and due to practical battery sizing constraints described in Sec. III-A.1. The selected final configuration $\mathcal{S}_f = (\mathcal{S}|m_{bat} = 3.5kg, b = 5.6m, \lambda = 18.5)$ has an overall estimated mass of $m_{tot} = 7.22kg$ and yields a predicted $t_{exc} = 7.89h$ and $t_{cm} = 8.38h$ for the nominal operating date and latitude.

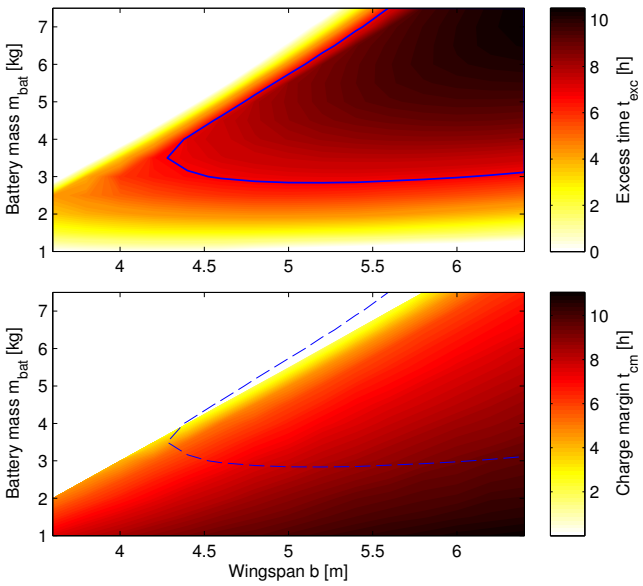

Fig. 3. Excess time t_{exc} (top) and charge margin t_{cm} (bottom) vs. optimization parameters b and m_{bat}, all at $\lambda = 18.5$. The configuration subset $\mathcal{S}$ satisfying $t_{exc} > t_{exc,req}$ under our design requirements lies inside the blue contour line.

TABLE I
FIXED PARAMETERS FOR THE CONCEPTUAL DESIGN

Parameter	Value	Description
eta_{sm}	0.20	Solar module efficiency
eta_{MPPT}	0.97	MPPT efficiency
eta_{prop}	0.58	Propulsion system effiency
e_{bat}	874800J/kg	Battery specific energy
f_{sm}	0.94	Solar module fill factor
k_{sm}	0.59kg/m	Solar module areal density
m_{av}	0.6kg	Avionics mass (including all cabling)
m_{pld}	0.1kg	Payload mass
P_{av}	4.5W	Avionics power consumption
P_{pld}	0.0W	Payload power consumption

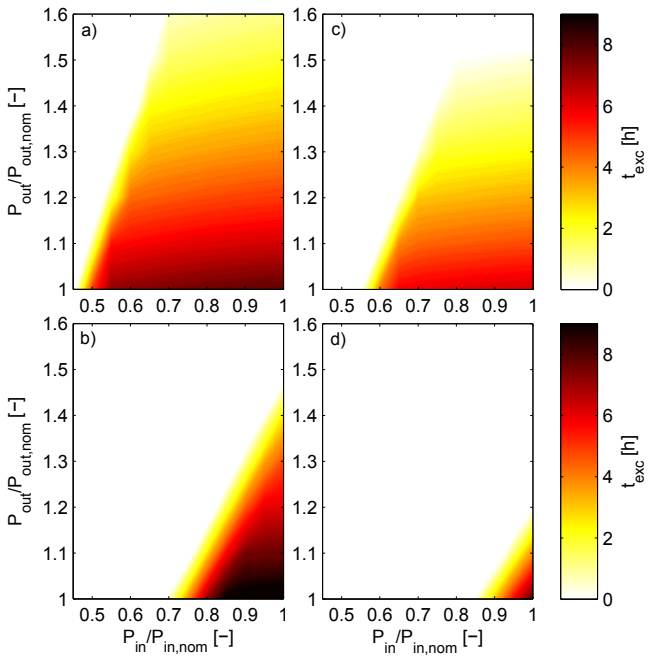

Fig. 4. Excess time t_{exc} under disturbed power input and output for the developed $b = 5.6m$, $\lambda = 18.5$ configuration: a) m_{bat}=3.5kg on June 21st b) $m_{bat} = 6.0kg$ on June 21st c) m_{bat}=3.5kg on April 21st d) $m_{bat} = 6.0kg$ on April 21st

D. Robustness analysis

To verify the multi-day flight robustness of the developed UAV configuration $\mathcal{S}_f$, we analyze its performance considering a set of local disturbances in UAV power input and output, namely

- The disturbed solar power income P_{solar}^{dist}, as caused by clouds or fog. Lacking knowledge of the exact spatial and temporal disturbance distribution, we assume the simple scaling

$$P_{solar}^{dist}(t) = P_{solar}^{nom}(t) \cdot k_{CCF}. \tag{7}$$

  Here, $k_{CCF} = [0, 1]$ represents the current cloud cover factor [**?**], i.e. the clearness of the atmosphere.
- The disturbed electrical power output P_{out}^{dist}. Wind downdrafts, head wind, or gusts may require increased propulsion or actuation power. Again, we assume

$$P_{out}^{dist}(t) = P_{out}^{nom}(t) \cdot k_{OPF}, \tag{8}$$

  with k_{OPF} representing the Output Power Factor.

Fig. 4 shows the remaining excess time with respect to these disturbances. The UAV configuration developed in section II-C (with $m_{bat} = 3.5kg$) still provides perpetual endurance with less than 50% of the solar power income or if more than 60% surplus power are required e.g. to compensate for downdrafts on June 21st (Fig.4a). In contrast, a configuation purely optimized towards excess time with $m_{bat} = 6.0kg$ (Fig.4b) will yield a higher maximum t_{exc} of 9.5h, however, the robustness with respect to clouds or higher required level power is greatly decreased. On April 21st, the UAV configuration of section II-C still provides solid robustness (Fig.4c), which verifies the $DoY^{nom} \pm$ 2 months perpetual endurance requirement. In contrast, the $m_{bat} = 6.0kg$ configuration (Fig.4d) can not provide reliable perpetual endurance anymore. Overall, the configuration developed using the extended optimization criteria from Sec. II-B thus shows significantly improved multi-day flight robustness in comparison with configurations that are purely optimized for maximum excess time.

TABLE II
ATLANTIKSOLAR DESIGN CHARACTERISTICS

Wing span	5.65m
Wing chord	0.305m
Length	2.03m
Height	0.45m
Mass	7.36kg
Battery mass	3.52kg
Wing loading	$4.28 \mathrm{kg/m^2}$
Stall speed	$8.1 \mathrm{m/s}$

III. DETAILED DESIGN AND REALIZATION

AtlantikSolar (Fig. 1) is a solar-powered Low-Altitude Long-Endurance(LALE) UAV designed and built at ETH Zurich for perpetual flight at $\varphi = 45$ geographical latitude from April 21st to August 21st. Although its design is mostly dictated by the requirement for low level-flight power consumption, it provides means to mount an advanced optical&infrared sensor pod developed at ETH Zurich for use in autonomous search and rescue or industrial inspection missions. The airplane airframe characteristics are summarized in table II. An overview over the airplane system topology is given in Fig. 6.

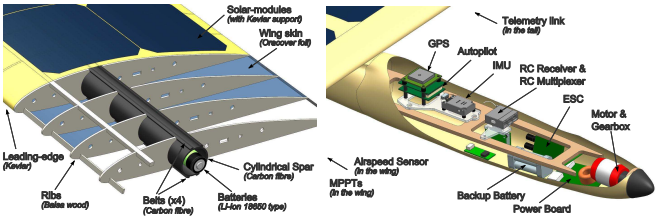

Fig. 5. Left: Wing structure with integrated batteries and solar cells. Right: Main avionics layout inside the airplane.

A. UAV Platform Design

1) Airframe: The structure of AtlantikSolar is built in a traditional rib-spar construction method (Fig. 5). The wing's main element is an inner cylindrical carbon-fibre spar to resist torsional wing loads. Four carbon-fibre belts of trapezoidal and laterally-varying cross-section are attached to the spar to optimally resist bending loads and to provide maximum wing stiffness to structurally unload the wing surface and especially the solar cells. The main wing can be disassembled into three wing pieces of $b < 2m$ each. The horizontal and vertical stabilizers are built as the main wing.

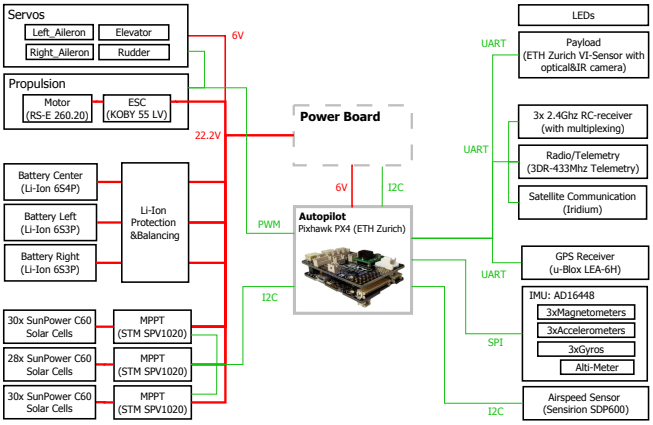

Fig. 6. AtlantikSolar system overview. For clarity, voltage lines from the autopilot to connected devices (5.0V and 3.3V) are omitted.

2) Energy Generation and Storage: The cylindrical wing spars are fitted with 72 cylindrical high energy-density industrial Lithium-Ion battery cells (Panasonic NCR18650b, 243Wh/kg) to optimally distribute the battery mass in a "span loader" concept. The cells are connected in a 6S (22.2V) configuration and provide $E_{bat,max} = 850Wh$ at $m_{bat} = 3.5kg$. The solar modules feature a total of 88 SunPower C60 cells with a measured module-level efficiency of $\eta_{sm} = 0.20$, an areal density of $k_{sm} = 590g/m^2$ and a maximum power output of 275W at $\varphi = 45$ on June 21st. Modules featuring SunPower E60 cells with a measured [**?**] $\eta_{sm} = 0.23$ are currently being integrated. The solar modules are seamlessly embedded in the upper wing surface to avoid premature flow separation.

3) Actuation: The propulsion system features a foldable custom built carbon-fibre propeller with diameter $D = 66cm$ and pitch $H = 60cm$. It is driven by a 5:1 reduction-ratio planetary gearbox, a RS-E Strecker 260.20 brushless DC motor with $k_V = 570RPM/V$ and a Kontronik Koby 55 LV motor controller at up to $P_{prop,max} = 450W$ electrical input power. The actuation system consists of four Volz DA-15N servos that drive the two ailerons, the all-moving elevator and the rudder. To guarantee reliable multi-day flight, the Volz actuators were successfully bench-tested throughout a simulated continuous 30-day flight [**?**].

4) Avionics: The avionics installation (Figs. 6 and 5) is centered around a Pixhawk PX4 Autopilot - an open source and open hardware project initiated at ETH Zurich - with a Cortex M4F microprocessor running at 168Mhz and featuring 192kB RAM. For attitude estimation (Sec. III-B.1), an ADIS 16448 10-axis Inertial Measurement Unit (IMU), a u-Blox LEA-6H GPS receiver, and a Sensirion SDP600 differential pressure sensor are used. The SDP600 airspeed sensor exhibits less than 5% error at airspeeds of 8m/s, which is essential to closely control the airspeed to the minimum required power P_{out} state. Both a 433Mhz medium-range telemetry link and a long-range IRIDIUM-based satellite backup link are integrated. The airplane implements a fully manual RC-command fall-back mode in case of a severe autopilot failure. Night operations are possible due to four on-board high-power indicator LEDs.

5) Payload: - VI Sensor [ref to VI-sensor paper; ref to Leutenegger thesis?] - 5 sentences + 1 picture

B. State Estimation and Control Design

1) State Estimation: - brief (5 sentence) description of SE type/principle - one verification plot (e.g. gps position "ground truth" vs. estimated position) then REF to stefan&Amir paper

2) System Identification: - System Identification & Modelling

Towards aiding the control synthesis procedure, a simplified linear state–space representation of the UAV dynamics was also derived based on recorded flight data and frequency–domain system identification methods. For non–aggressive maneuvering and around level flight, linear models may capture the vehicle response for small perturbations around a given equilibrium. Decoupling the longitudinal and lateral axis the dynamics of a UAV may take the following form [**?**], [**?**]:

$$\begin{aligned} \mathbf{M}_{lon}\dot{\mathbf{x}}_{lon} &= \mathbf{A}'_{lon}\mathbf{x}_{lon} + \mathbf{B}'_{lon}u_{elev} \\ \mathbf{x}_{lon} &= [u\ w\ q\ \theta]^T \end{aligned} \tag{9}$$

where u, w, q, θ correspond to the body x–axis, z–axis velocities, the pitch rate and the pitch angle respectively, u_{elev} corresponds to the elevator deflection and

$$\mathbf{M}_{lon} = \begin{bmatrix} m & 0 & 0 & 0 \\ 0 & m & 0 & 0 \\ 0 & 0 & I_y & 0 \\ 0 & 0 & 0 & 1 \end{bmatrix}, \tag{10}$$

$$\mathbf{A}'_{lon} = \begin{bmatrix} X_u & X_w & X_q - mW_e & -mg\cos\theta_e \\ Z_u & Z_w & Z_q + mU_e & -mg\sin\theta_e \\ M_u & M_w & M_q & 0 \\ 0 & 0 & 1 & 0 \end{bmatrix} \mathbf{B}'_{lon} = \begin{bmatrix} X_{u_{elev}} \\ Z_{u_{elev}} \\ M_{u_{elev}} \\ 0 \end{bmatrix}$$

where m is the mass, I_y the inertia around the body y–axis, W_e, θ_e are the trimming points of vertical velocity and pitch angle, and the elements of $\mathbf{M}_{lon}, \mathbf{A}'_{lon}$ and $\mathbf{B}'_{lon}$ form the stability and control derivatives of the UAV longitudinal dynamics.

Similarly, for the lateral dynamics the model takes the following form:

$$\begin{aligned} \mathbf{M}_{lat}\dot{\mathbf{x}}_{lat} &= \mathbf{A}'_{lat}\mathbf{x}_{lat} + \mathbf{B}'_{lat}u_{elev} \\ \mathbf{x}_{lat} &= [v\ p\ r\ \phi]^T \end{aligned} \tag{11}$$

where v, p, r, ϕ correspond to the body y–axis velocity, the roll and yaw rates and roll angle respectively, u_{ail} is the aileron deflection, u_{rud} is the rudder deflection and

$$\mathbf{M}_{lat} = \begin{bmatrix} m & 0 & 0 & 0 \\ 0 & I_x & -I_{xz} & 0 \\ 0 & -I_{xz} & I_z & 0 \\ 0 & 0 & 0 & 1 \end{bmatrix}, \tag{12}$$

$$\mathbf{A}'_{lat} = \begin{bmatrix} Y_v & Y_p + mW_e & Y_r - mU_e & mg\cos\theta_e \\ L_v & L_p & L_r & 0 \\ N_v & N_p & N_r & 0 \\ 0 & 1 & \tan\theta_e & 0 \end{bmatrix}, \mathbf{B}'_{lat} = \begin{bmatrix} Y_{u_{ail}} & Y_{u_{rud}} \\ L_{u_{ail}} & L_{u_{rud}} \\ N_{u_{ail}} & N_{u_{rud}} \\ 0 & 0 \end{bmatrix}$$

where I_x the inertia around the body x–axis, I_{xz} the cross–inertia term of the body x, z–axes and the elements of

$\mathbf{M}_{lat}, \mathbf{A}'_{lat}$ and $\mathbf{B}'_{lat}$ form the stability and control derivatives of the UAV lateral dynamics.

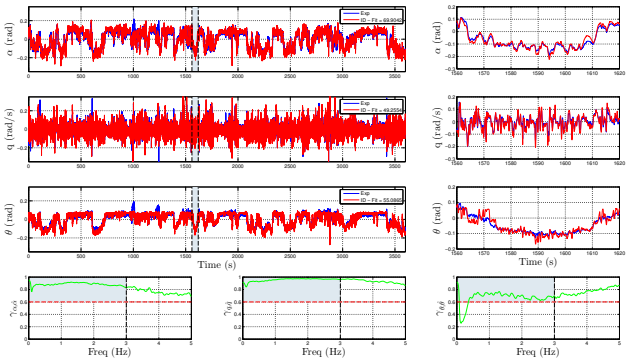

Fig. 7. Longitudinal subsystem system identification validation plot.

3) Control: Currently implemented control scheme: - Control using SAS and CAS PID inner loops - limiters - airspeed and error gain scheduling - coordinated turn control - aircraft trims - overspeed protection - (SPRC) - TECS altitude and airspeed control - Thermal compliance mode - hMax/hMin protection - spoilers on/off auto - (Altitude Ramps) - L1 non-linear guidance waypoint following - gain adaption to account for windy conditions (low ground speed- ¿....) - good performance on PX4 -¿ mention cpu load

- Generic/modular control scheme: PID implemented as baseline approach, but MPC already tested[REF OMLAS], LPV-MPC in development, Failure tolerant controller tested using same approach[REF MASTER THESIS]. - Full pre-flight verification in HIL before going into flight tests - Test at what winds and what performance (e.g. during loitering for power measurements -¿ very good tracking) - Later: show waypoint tracking (not loitering!) with altitude change for control (&State Estimator) operation verification. Alternatively: Show this in the ICARUS test paths ...

IV. EXPERIMENTAL RESULTS

- mention total flight hours, total flights. Mention that 2 AtlantikSolars have already been built & flown. Range of weather conditions?

A. Subsystem level results

- power efficiency curves. P_level from Test flights. Comparison to conceptual design. Describe why power consumption not optimal: e.g. because optimal CD/CLÎ.5 assumed, but this has a) to be met in average and b) even then fluctuations as seen in flight tests are on the order of 2-3 degrees in AOA or +/- 1m/s, so this will never be met perfectly. - solar system operation and recharge of batteries - state estimation (if not shown before) - control (if not shown before): - SE&Control: PID performance over various trim points. PID computational requirements (low!)

B. Continuous 12hour Flight

- focus on battery performance. Say that even more possible (mention some results from the lab tests) - explain how much autonomous, under which conditions.

C. Mapping Flights in Search and Rescue scenarios

- mapping missions in ICARUS. - REF to Separate paper??? Yes, but only once both are accepted. - some cool pics/reconstructed maps

V. CONCLUSIONS

Mention: - Main lessons learned / summarize main points of paper - Future work

APPENDIX

Appendixes should appear before the acknowledgment.

ACKNOWLEDGMENT

The preferred spelling of the word acknowledgment in America is without an e after the g. Avoid the stilted expression, One of us (R. B. G.) thanks . . . Instead, try R. B. G. thanks. Put sponsor acknowledgments in the unnumbered footnote on the first page.